Journal of Materials Chemistry B

PAPER

View Article Online
View Journal | View Issue

Cite this: J. Mater. Chem. B, 2018, 6, 7439

Selective tracking of ovarian-cancer-specific γ-glutamyltranspeptidase using a ratiometric two-photon fluorescent probe†

Ben Shi,‡[a] Zhenyu Zhang,‡[a] Qingqing Jin,‡[b] Zhiqiang Wang,[c] Jie Tang,[a] Ge Xu,[a] Tianli Zhu,[a] Xueqing Gong,[c] Xinjing Tang*[b] and Chunchang Zhao*[a]

Received 3rd July 2018,
Accepted 4th October 2018

DOI: 10.1039/c8tb01735b

rsc.li/materials-b

Real-time tracking of GGT enzymatic activity in human ovarian cancer cells is a reliable method for accurate prediction of cancer diagnosis and management. Here, we report the two-photon ratiometric tracking of GGT activity in cancer cells based on a probe with switchable Förster resonance energy transfer properties. In the absence of GGT, the designed probe showed two well-resolved emission bands at 461 and 610 nm, corresponding to the 7-hydroxycoumarin donor and BODIPY acceptor, respectively. In contrast, GGT catalyzed cascade reactions including cleavage of the γ-glutamyl group and subsequent aromatic hydrocarbon transfer from the S to N atom increased the distance between the two chromophores, thus decreasing the FRET efficiency, with the recovery of the donor fluorescence at 461 nm. By exploiting this enzyme-triggered ratiometric measurement, successful differentiation of ovarian cancer cells from normal cells with this probe was realized by two-photon fluorescence confocal microscopy.

Introduction

Ovarian cancer is one of the most common tumors in women and accounts for a major cause of cancer death.[1] Primary cytoreductive surgery is vital to the treatment of women with ovarian carcinoma.[2] Since successful surgical management crucially relies on the precise localization of cancerous tissues, measurement of ovarian-cancer-related biomarkers assisted by molecular imaging probes will improve surgical prognosis.[3] Among many studied biomarkers, γ-glutamyltranspeptidase (GGT) has been reported to express at high levels in human ovarian cancers.[4–6] GGT, a cell-membrane-bound enzyme, catalyzes the metabolism of GSH, wherein a complementary supply of cysteine is provided, thus conferring the advantage for tumorigenesis and invasion.[7] Real-time tracking of GGT enzymatic activity in human cancer cells should thus be a reliable method for accurate prediction of cancer diagnosis and management.

Indeed, a number of analytical methods have been explored for GGT assays to better understand GGT-related pathological sequences, including high-performance liquid chromatography (HPLC), and colorimetric and fluorescent assays.[8] Because of their operational simplicity, spatiotemporal resolution and noninvasive features, fluorescent probes and sensors have attracted intense interest.[9–14] Accordingly, several fluorescent probes for GGT detection have been developed based on the GGT-catalyzed cleavage of the γ-glutamyl bond.[15–25] However, many reported sensing systems are still subject to limitations concerning a fluorescence turn-on response with a single detection signal. As is known, fluorescence turn-on signals heavily depend on experimental conditions such as probe concentration and excitation intensity.[26–29] In sharp contrast, ratiometric probes can eliminate adverse effects and provide quantitative measurements of biomolecules.[30–34] Recently, we and others have reported two such ratiometric probes for GGT activity assay.[35,36] However, the shallow penetration depth of the short excitation wavelength restricts their practical applications. As an alternative and innovative strategy, designing two-photon excitation (TPE) probes with ratiometric imaging should address the above mentioned issues. TPE, utilizing two near-IR photons as the excitation source, endows the advantages of deep tissue penetration, minimum photodamage to biosamples, and low background fluorescence.[37,38] However, to the best of our knowledge, no ratiometric probes with two-photon excitation for GGT assay have been reported yet.

[a] Key Laboratory for Advanced Materials and Institute of Fine Chemicals, School of Chemistry and Molecular Engineering, East China University of Science & Technology, Shanghai 200237, P. R. China. E-mail: zhaocchang@ecust.edu.cn
[b] State Key Laboratory of Natural and Biomimetic Drugs, School of Pharmaceutical Sciences, Peking University, Beijing, 100191, China. E-mail: xinjingt@bjmu.edu.cn
[c] Key Laboratory for Advanced Materials, Centre for Computational Chemistry and Research Institute of Industrial Catalysis, School of Chemistry and Molecular Engineering, East China University of Science and Technology, 130 Meilong Road, Shanghai, 200237, P. R. China

† Electronic supplementary information (ESI) available: Procedures for synthesis, characterization data, and supplementary figures. See DOI: 10.1039/c8tb01735b

‡ These authors contributed equally to this work.

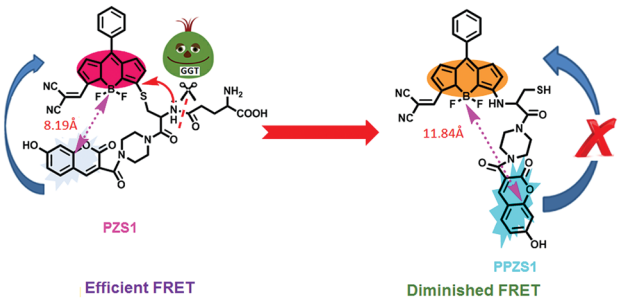

Scheme 1 GGT switchable FRET in the designed probe **PZS1** and its conversion to **PPZS1**.

In this contribution, we reported the two-photon ratiometric detection of cancer cells by tracking GGT activity based on a probe with switchable Förster resonance energy transfer properties (Scheme 1). In our design, 7-hydroxycoumarin is expected to act as an energy donor and a BDIPIY derivative as an energy acceptor. In the free probe, the two fluorophores are installed in close proximity to each other and FRET from the 7-hydroxycoumarin to BODIPY chromophore occurs efficiently, affording two well-resolved emission bands at 461 and 610 nm. Upon interaction with GGT, the cleavage of the γ-glutamyl group and subsequent aromatic hydrocarbon transfer from the S to N atom lead to the unfavorable arrangement of the two fluorophores (increasing the distance between the two chromophores), thus decreasing the FRET efficiency, with the recovery of the donor fluorescence at 461 nm. By means of this enzyme-triggered ratiometric measurement, this probe successfully demonstrated its capability for differentiation of ovarian cancer cells from normal cells by two-photon fluorescence confocal microscopy.

Results and discussion

The synthetic procedures for probe **PZS1** are depicted in Scheme 2. In brief, treatment of 5-(*tert*-butoxy)-4-((*tert*-butoxycarbonyl)amino)-5-oxopentanoic acid with *N*-hydroxysuccinimide (NHS) and 1-ethyl-3-(3-dimethylaminopropyl)-carbodiimide hydrochloride (EDC) in CH_2Cl_2 led to the production of an activated intermediate, which was coupled to *S*-trityl-L-cysteine to afford the Gly-Cys peptide. Subsequently, this peptide was conjugated to 7-hydroxylcoumarin *via* a piperazine linkage by a standard coupling reaction to provide compound **5**, which was then subjected to sequential deprotection with TFA (trifluoroacetic acid) and TES (triethylsilane) to produce compound **6**. Finally, the probe **PZS1** was obtained by the aromatic nucleophilic substitution reaction between **6** and BODIPY *via* the formation of a thioether bond. The chemical structures of the new compounds were fully characterized by ^{1}H NMR, ^{13}C NMR and HRMS.

The fluorescence response of **PZS1** to GGT was first evaluated in aqueous buffer (0.01 mM PBS, pH 7.4). In the absence of GGT, **PZS1** shows intense absorption at 358 nm and 538 nm (Fig. 1a), derived from the 7-hydroxylcoumarin and BODIPY chromophore, respectively. Upon excitation at 350 nm, two well-resolved emission bands were noted at 461 nm and 610 nm for the free **PZS1**

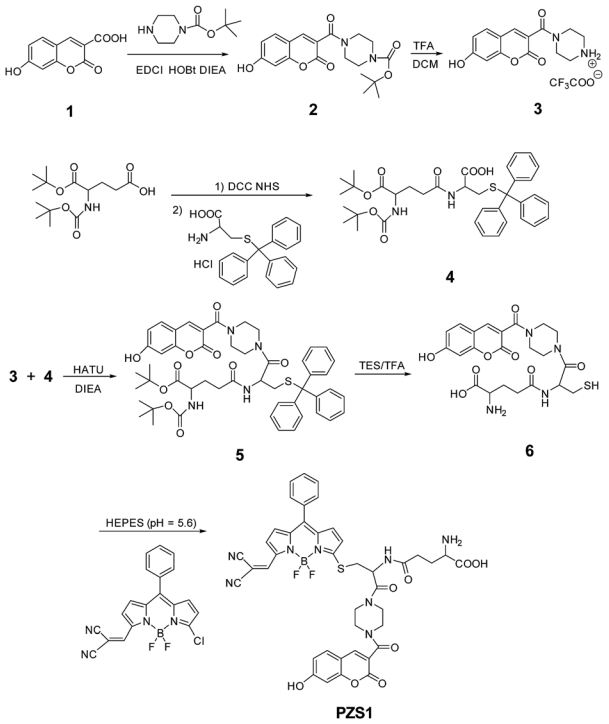

Scheme 2 Synthesis of **PZS1**.

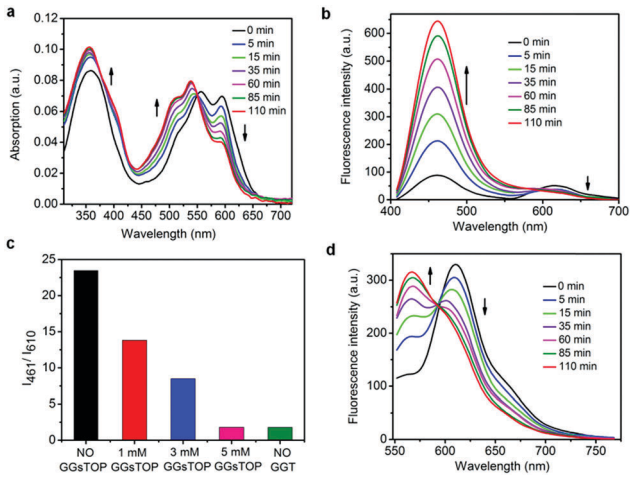

Fig. 1 Time-dependent absorption (a) and fluorescence (b) spectral changes of **PZS1** (10 μM) in the presence of GGT (600 U L^{-1}). λ_{ex} = 350 nm. (c) The fluorescence intensity ratio (I_{461}/I_{610}) of **PZS1** (10 μM) when GGT was pretreated with various concentrations of GGsTOP before treatment with the probe for 110 min. (d) Time dependent fluorescence changes of the BODIPY unit in **PZS1** after the addition of GGT (600 U L^{-1}). λ_{ex} = 510 nm.

(Fig. 1b), with a FRET efficiency of 88.8% (Fig. S1, ESI†), and the solution of probe **PZS1** showed a pink fluorescence. Upon addition of GGT (600 U L^{-1}), the emission band at 461 nm exhibited a dramatic enhancement accompanied by a decrease of the emission at 610 nm, and the fluorescence color of the solution was bluish green (Fig. S2, ESI†). Notably, a 23.5-fold enhancement of the fluorescence intensity ratio (I_{461}/I_{610}) was observed (Fig. 1c),

which indicated that **PZS1** can serve as a potent ratiometric probe. In contrast, the ratiometric fluorescence change was reduced when the GGT was pretreated with GGsTOP (Fig. S3, ESI†), an inhibitor of GGT, before treatment with probe **PZS1**. The reduction was GGsTOP dose-dependent. The intensity ratio (I_{461}/I_{610}) decreased from 23.5 to 13.8, 8.5 and 1.8, respectively, after pretreatment with 1 mM, 3 mM and 5 mM GGsTOP, indicating that GGT is vital for triggering the FRET-based ratiometric fluorescence signal change. According to our previous studies,[35] GGT can catalyze the cleavage of the γ-glutamyl bond, which was followed by the aromatic hydrocarbon transfer reaction between the sulfur and the nitrogen atom in BODIPY, leading to obvious fluorescence variations.[39,40] In the case of **PZS1**, such GGT-induced translation was demonstrated by observation of the optical changes of BODIPY. As expected, a dramatic decrease in the emission of **PZS1** at 610 nm was afforded in the presence of GGT, along with a simultaneous buildup of an emission at 567 nm corresponding to amino-substituted BODIPY (Fig. 1d). This result confirmed that GGT triggered the transformation from **PZS1** (sulfur-substituted BODIPY) to amino-substituted BODIPY. HRMS analysis was also used to confirm this reaction process. The peak of our proposed amino-substituted BODIPY (m/z = 719.2021, $[M + H]^+$) was clearly manifested (Fig. S4, ESI†).

Obviously, the GGT-triggered transformation reaction contributed to the switchable FRET process and the recovery of the donor fluorescence at 461 nm. To gain a deep understanding of the FRET, theoretical calculations using density functional theory (DFT) with G09 and B3LYP/6-311G were carried out. Based on the optimized chemical structures of **PZS1** and **PPZS1**, the distance between the coumarin and BODIPY chromophore was estimated to be 8.19 Å and 11.84 Å, respectively (Fig. 2). It is known that the energy transfer efficiency is inversely proportional to the sixth power of the distance between the donor and acceptor, and increasing the distance will rapidly lead to a decrease of energy-transfer efficiency. GGT-triggered conversion of **PZS1** to **PPZS1** increases the distance between coumarin and BODIPY, presumably contributing to the switchable FRET process.

The selective response of **PZS1** to GGT activity was then tested. The data in Fig. 3 indicated that **PZS1** exhibited negligible change in the fluorescence ratio (I_{461}/I_{610}) upon treatment with potential interfering species, including glucoamylase, aprotinin, collagen hydrolase, phosphatase, lipase, human plasma, FBS and inorganic salts (KCl, $MgCl_2$, $CaCl_2$, $ZnCl_2$, $FeCl_2$, $FeCl_3$, and $MnCl_2$).

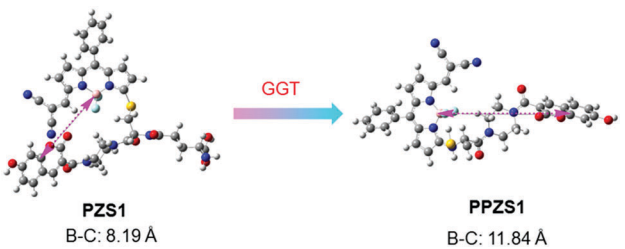

Fig. 2 The optimized chemical structures of **PZS1** and **PPZS1** by theoretical calculations using density functional theory (DFT) with G09 and B3LYP/6-311G.

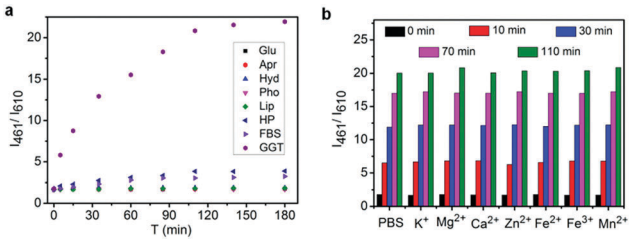

Fig. 3 (a) The fluorescence intensity ratio (I_{461}/I_{610}) changes in the presence of potential interfering species including collagen hydrolase, phosphatase, aprotinin, glucoamylase, 10% FBS or 10% human plasma. (b) The effects of some important metal ions on the responsive process of **PZS1** (10 μM) to GGT (600 U L^{-1}).

However, a dramatic enhancement was noted when treated with GGT, suggesting that **PZS1** has sufficient selectivity for application. Notably, fluorescence titration experiments showed that the fluorescence ratio (I_{461}/I_{610}) change of **PZS1** is GGT dose-dependent within a concentration range from 0 to 800 U L^{-1} (Fig. S5, ESI†). Utilizing the Michaelis–Menten equation, the kinetic values of **PZS1** against GGT were then estimated. The K_m and V_{max} values were calculated to be 0.75 μM min^{-1} and 18.62 μM, respectively (Fig. S6, ESI†).

Having established the specificity of **PZS1** for monitoring GGT activity in aqueous solutions, we then explored the capability of **PZS1** for differentiating ovarian cancer cells from normal cells *via* living-cell tracking of GGT activity. The feasibility of this probe

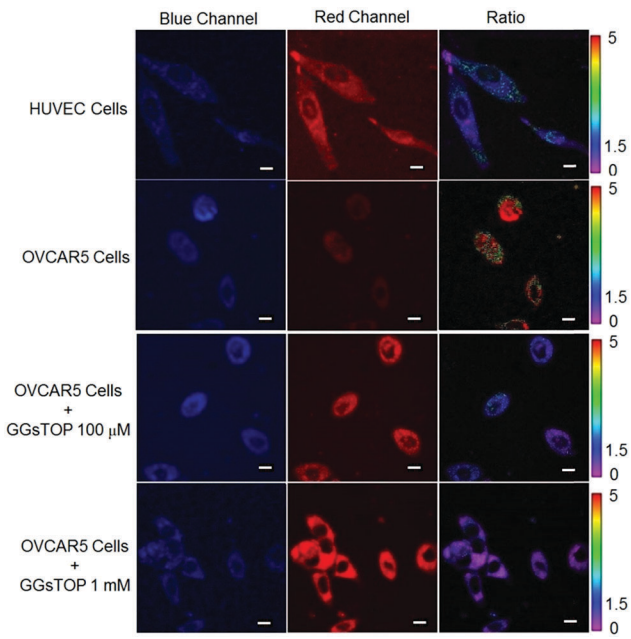

Fig. 4 Differentiation of ovarian cancer cells from normal cells *via* living-cell tracking of GGT activity with **PZS1** (10 μM). For imaging of HUVEC cells or OVCAR5 cells, these cells were incubated with **PZS1** (10 μM) for 30 minutes. For assaying the inhibitory effect of GGsTOP, ovarian cancer cells were pretreated with GGsTOP for 30 minutes and then loaded with **PZS1** (10 μM) for 30 minutes. The excitation wavelength was 700 nm and the emission was collected at 400–500 nm (blue channel) and 600–650 nm (red channel); the ratio image was generated from the blue to red channel. The scale bar is 10 μm.

for differentiation was investigated using two-photon microscopy (TPM) with TP excitation at 700 nm. As shown in Fig. 4, OVCAR5 cells labeled with **PZS1** under excitation for 30 min showed strong fluorescence in the blue channel but negligible fluorescence in the red channel with an average emission ratio (I_{blue}/I_{red}) of 4.52 (Fig. S7, ESI†). However, the signal ratio decreased when the cells were pretreated with GGsTOP before incubation with probe **PZS1**. The ratio decreased from 4.52 to 1.34 and 0.81, respectively, after addition of 100 μM and 1 mM GGsTOP. Notably, I_{blue}/I_{red} was time-dependent (Fig. S8, ESI†); for example, OVCAR5 cells incubated with **PZS1** for 15 min, 30 min, 45 min and 1 h led to ratiometric ratios of 3.5, 4.6, 4.5 and 4.4, respectively, indicative of the enzyme-mediated transformation from **PZS1** to amino-substituted BODIPY in transmembrane domains.[35] These results clearly demonstrate that **PZS1** is capable of tracking GGT levels in living cells using TPM. As is known, human umbilical vein endothelial cells (HUVECs) express negligible GGT; thus HUVECs stained with **PZS1** should exhibit a decreased I_{blue}/I_{red} ratio when compared to ovarian cancer cells. As expected, the emission ratio in HUVECs was reduced to around 1.22. In addition, prolonging the treatment of HUVECs with **PZS1** showed no obvious I_{blue}/I_{red} change. These results firmly evidenced the capability of **PZS1** for differentiation of ovarian cancer cells from normal cells by tracking GGT activity.

Conclusions

In conclusion, we have developed a switchable FRET probe for assaying GGT activity that induces aromatic hydrocarbon transfer from the S to N atom in the BODIPY unit of this probe, increasing the distance between the donor and acceptor and thus modulating the FRET. Utilizing GGT-triggered ratiometric responsiveness, this probe was successfully applied to monitor GGT activity in living cells by two-photon fluorescence confocal microscopy, which illustrated that the probe is capable of differentiating ovarian cancer cells from normal cells by tracking GGT activity.

Conflicts of interest

The authors declare no competing financial interest.

Acknowledgements

We gratefully acknowledge the financial support from the National Science Foundation of China (grant number 21672062).

Notes and references

1 I. Vergote, C. G. Tropé, F. Amant, G. B. Kristensen, T. Ehlen, N. Johnson, R. H. M. Verheijen, M. E. L. van der Burg, A. J. Lacave, P. B. Panici, G. G. Kenter, A. Casado, C. Mendiola, C. Coens, L. Verleye, G. C. E. Stuart, S. Pecorelli and N. S. Reed, *N. Engl. J. Med.*, 2010, **363**, 943.
2 C. T. Griffiths and A. F. Fuller, *Surg. Clin. North Am.*, 1978, **58**, 131.
3 Y. Liu, J. Tan, Y. Zhang, J. Zhuang, M. Ge, B. Shi, J. Li, G. Xu, S. Xu, C. Fan and C. Zhao, *Biomaterials*, 2018, **173**, 1.
4 M. H. Hanigan, H. F. Frierson Jr., J. E. Brown, M. A. Lovell and P. T. Taylor, *Cancer Res.*, 1994, **54**, 286.
5 A. Pompella, V. D. Tata, A. Paolicchi and F. Zunino, *Biochem. Pharmacol.*, 2006, **71**, 231.
6 D. Yao, D. Z. Huang, J. Lu, Q. Tao, Z. Yu and X. Meng, *Cancer*, 2000, **88**, 761.
7 A. Pompella, V. De Tata, A. Paolicchi and F. Zunino, *Biochem. Pharmacol.*, 2006, **71**, 231.
8 Y. Urano, M. Sakabe, N. Kosaka, M. Ogawa, M. Mitsunaga, D. Asanuma, M. Kamiya, M. R. Young, T. Nagano, P. L. Choyke and H. Kobayashi, *Sci. Transl. Med.*, 2011, **3**, 110.
9 T. Kowada, H. Maeda and K. Kikuchi, *Chem. Soc. Rev.*, 2015, **44**, 4953.
10 M. Vendrell, D. Zhai, J. C. Er and Y. T. Chang, *Chem. Rev.*, 2012, **112**, 4391.
11 J. Chan, S. C. Dodani and C. J. Chang, *Nat. Chem.*, 2012, **4**, 973.
12 D. Wu, A. C. Sedgwick, T. Gunnlaugsson, E. U. Akkaya, J. Yoon and T. D. James, *Chem. Soc. Rev.*, 2017, **46**, 7105.
13 M. H. Lee, A. Sharma, M. J. Chang, J. J. Lee, S. Son, J. L. Sessler, C. Kang and J. S. Kim, *Chem. Soc. Rev.*, 2018, **47**, 28.
14 L. Wu and X. G. Qu, *Chem. Soc. Rev.*, 2015, **44**, 2963.
15 L. H. Li, W. Shi, Z. Wang, Q. Y. Gong and H. M. Ma, *Anal. Chem.*, 2015, **87**, 8353.
16 X. F. Hou, F. Zeng and S. Z. Wu, *Biosens. Bioelectron.*, 2016, **85**, 317.
17 T. Nishihara, H. A. I. Yoshihara, H. Nonaka, Y. Takakusagi, F. Hyodo, K. Ichikawa, E. Can, J. A. M. Bastiaansen, Y. Takado, A. Comment and S. Sando, *Angew. Chem., Int. Ed.*, 2016, **55**, 10626.
18 M. Chiba, Y. Ichikawa, M. Kamiya, T. Komatsu, T. Ueno, K. Hanaoka, T. Nagano, N. Lange and Y. Urano, *Angew. Chem., Int. Ed.*, 2017, **56**, 10418.
19 H. J. Tong, Y. J. Zheng, L. Zhou, X. M. Li, R. Qian, R. Wang, J. H. Zhao, K. Y. Lou and W. Wang, *Anal. Chem.*, 2016, **88**, 10816.
20 S. Park, S. Y. Lim, S. M. Bae, S. Y. Kim, S. J. Myung and H. J. Kim, *ACS Sens.*, 2016, **1**, 579.
21 S. Li, R. Hu, C. L. Yang, X. Zhang, Y. Zeng, S. Q. Wang, X. D. Guo, Y. Li, X. P. Cai, S. R. Li, C. W. Han and G. Q. Yang, *Biosens. Bioelectron.*, 2017, **98**, 325.
22 Z. J. Hai, J. J. Wu, L. Wang, J. C. Xu, H. F. Zhang and G. L. Liang, *Anal. Chem.*, 2017, **89**, 7017.
23 J. Tian, Q. L. Yan, Y. Zhu, J. C. Zhang, J. Li, B. Shi, G. Xu, C. H. Fan and C. C. Zhao, *Chin. J. Chem.*, 2017, **35**, 1711.
24 X. F. Hou, Q. X. Yu, F. Zeng, C. M. Yu and S. Z. Wu, *Chem. Commun.*, 2014, **50**, 3417.
25 P. S. Zhang, X. F. Jiang, X. Z. Nie, Y. Huang, F. Zeng, X. T. Xia and S. Z. Wu, *Biomaterials*, 2016, **80**, 46.
26 M. G. Ren, K. Zhou, L. W. He and W. Y. Lin, *J. Mater. Chem. B*, 2018, **6**, 1716.
27 L. Y. Niu, Y. Z. Chen, H. R. Zheng, L. Z. Wu, C. H. Tung and Q. Z. Yang, *Chem. Soc. Rev.*, 2015, **44**, 6143.
28 Z. G. Song, Y. N. Hong, R. T. K. Kwok, J. W. Y. Lam, B. Liu and B. Z. Tang, *J. Mater. Chem. B*, 2014, **2**, 1717.

29 Z. Ye, C. Duan, Q. Hu, Y. Zhang, C. Q. Qin and L. T. Zeng, *J. Mater. Chem. B*, 2017, **5**, 3600.
30 B. Shi, X. F. Gu, Z. J. Wang, G. Xu, Q. Fei, J. Tang and C. C. Zhao, *ACS Appl. Mater. Interfaces*, 2017, **9**, 35588.
31 C. Zhao, X. Zhang, K. Li, S. Zhu, Z. Guo, L. Zhang, F. Wang, Q. Fei, S. Luo, P. Shi, H. Tian and W.-H. Zhu, *J. Am. Chem. Soc.*, 2015, **137**, 8490.
32 G. Xu, Q. Yan, X. Lv, Y. Zhu, K. Xin, B. Shi, R. Wang, J. Chen, W. Gao, P. Shi, C. Fan, C. Zhao and H. Tian, *Angew. Chem., Int. Ed.*, 2018, **57**, 3626.
33 F. Wang, G. Xu, X. Gu, Z. Wang, Z. Wang, B. Shi, C. Lu, X. Gong and C. Zhao, *Biomaterials*, 2018, **159**, 82.
34 Z. S. Wu and X. J. Tang, *Anal. Chem.*, 2015, **87**, 8613.
35 F. Y. Wang, Y. Zhu, L. Zhou, L. Pan, Z. F. Cui, Q. Fei, S. L. Luo, D. Pan, Q. Huang, R. Wang, C. C. Zhao, H. Tian and C. H. Fan, *Angew. Chem., Int. Ed.*, 2015, **54**, 7349.
36 S. Park, D. J. Bae, Y. M. Ryu, S. J. Myung and S. J. Kim, *Chem. Commun.*, 2016, **52**, 10400.
37 F. Helmchen and W. Denk, *Nat. Methods*, 2005, **2**, 932.
38 W. R. Zipfel, R. M. Williams and W. W. Webb, *Nat. Biotechnol.*, 2003, **21**, 1369.
39 L. Y. Niu, Y. S. Guan, Y. Z. Chen, L. Z. Wu, C. H. Tung and Q. Z. Yang, *J. Am. Chem. Soc.*, 2012, **134**, 18928.
40 F. Wang, L. Zhou, C. Zhao, R. Wang, Q. Fei, S. Luo, Z. Guo, H. Tian and W.-H. Zhu, *Chem. Sci.*, 2015, **6**, 2584.